Co-Simulation Stability in Power Systems

Thainan Santos Theodoro
Federal University of Ouro Preto
João Monlevade, Brazil
thainan.theodoro@ufop.edu.br

Marcelo Aroca Tomim
Federal University of Juiz de Fora
Juiz de Fora, Brazil
marcelo.tomim@ufjf.br

Pedro Gomes Barbosa
Federal University of Juiz de Fora
Juiz de Fora, Brazil
pedro.gomes@ufjf.br

***Abstract*—This study focuses on dynamic modeling in power system co-simulation and aims to develop a state space mathematical model to evaluate the impact of phasor extraction, communication methods and system equivalent impedance on co-simulation stability. A 2-bus test power system with RLC load and a continuous-time pi model transmission line is used to validate the developed methodology. The results highlight the importance of a robust interface bar in enhancing stability and caution against extreme power values that can induce instability in simulation process. Overall, this work contributes to the study of the stability of power system co-simulation, considering different phasor extraction methods, communication protocols and complex systems, thus advancing the research and development of co-simulation technology.**

***Index Terms*—Co-simulation; Stability; Transient Stability; Electromagnetic transients; Power Systems.**

I. Introduction

Co-simulating Transient Stability (TS) and Electromagnetic Transients (EMT) programs is a valuable approach for assessing new equipment integration in modern power systems. It combines fast TS calculations with precise EMT accuracy. However, challenges arise in terms of accuracy and stability when incorporating various phasor extraction methods and communication protocols into mathematical modeling, despite the availability of tools like PSCAD-PSS/E, OpenHybridSim, DIgSILENT, and ePHASORSIM-eMEGASIM in the market[1], [2].

It is crucial to distinguish between system stability and co-simulation stability. System stability pertains to the ability of a power system to maintain dynamic equilibrium despite internal conditions and configurations, including power system devices and control loops. On the other hand, co-simulation stability concerns the integration of systems, influenced by factors like communication protocols, phasor extraction, and equivalent circuits. It's worth noting that while system stability is important, it doesn't guarantee co-simulation stability.

Co-simulation faces stability challenges due to model differences, phasor extraction, and communication protocols. It involves key variables like power, voltage, and current, demanding precise phasor extraction methods such as Discrete Fourier Transform (DFT), Least-Square Curve Fitting (LSCF) [3], and Second-Order Generalized Integrator-Time Varying Phase-locked loop (SOGI-TVP) [4]. TS and EMT simulations have discrepant time-step sizes (expressed as a substantial H/h ratio), requiring consideration of data extrapolation between communication instances and time delays introduced by communication protocols, whether serial or parallel.

In recent years, co-simulation in electrical systems has garnered attention from the scientific community. However, most studies focus either on (*i*) various applications [5], [6] or (*ii*) on the accuracy of results, varying equivalent circuits, communication protocols, phasor extraction, etc. [7]. In this context, few works aim to investigate the stability of co-simulation in electrical systems, despite this topic having gained recent attention [8], [9], [10]. One of the earliest attempts to understand the stability of co-simulation regarding the phasor extraction method was made by [9]. In this approach, the model was simplified and did not consider the effects of communication. In contrast, this study presents a method for modeling co-simulation in the frequency domain, observing the impacts (*i*) of phasor extraction methods such as DFT, LSCF, and SOGI-TVP, as well as (*ii*) the delays caused by communication between the TS and EMT programs. This approach aims for a better understanding of co-simulation stability, enhancing its reliability and precision in Power Systems analysis.

Various methods exist in the literature for phasor extraction in co-simulation. In [11], the abc to dq coordinate transformation was applied, primarily suited for balanced three-phase systems. Another approach involvesDynamic Phasor (DP), as discussed in [3] and [12]. In general, the concepts of (i) Fast Time-Varying Phasors [13], (ii) Generalized Averaging Method [14], (iii) Shifted-Frequency Analysis [15], and (iv) Base-Frequency Dynamic Phasors [16] are very similar and extract time-varying Fourier coefficients from the signal. While these dynamic phasor extraction methods hold significance, this work does not delve into their detailed modeling and discussion.

Motivation and contribution of the work

This study focuses on investigating co-simulation stability within Electrical Power Systems. Its objectives encompass (*i*) identifying critical stability parameters, (*ii*) analyzing the dynamic behavior of various phasor extraction methods, (*iii*) evaluating the impact of sampling effects and interface delays, and (*iv*) providing guidance for selecting suitable phasor extraction methods in EMT-TS co-simulation. The ultimate

Submitted to the 23rd Power Systems Computation Conference (PSCC 2024).

aim is to enhance co-simulation's stability and accuracy in Electrical Power Systems analysis, contributing to a better understanding of power system phenomena. It is worth noting that the focus of this work is to investigate how the phasor extraction method contributes to the stability of co-simulation. Other topics have not yet been investigated with this methodology, such as the choice of equivalent circuit or the location of the interface bus. Furthermore, given that stability analysis is our primary focus, this work does not delve into the accuracy of the models. Instead, another investigation specifically addresses the precision aspect of co-simulation [17].

Overall, this research enhances co-simulation stability analysis methodology. It has been validated through numerical tests, highlighting that improper selection of phasor extraction methods or communication protocols can destabilize an inherently stable system. The proposed generic methodology can be applied to assess stability across various phasor extraction techniques, communication protocols, and complex systems, thus advancing co-simulation technology research and development.

The paper's structure is as follows: Section II details the methodology for mathematically modeling co-simulation in the frequency domain; following, Section III presents the analysis outcomes based on these models; lastly, Section IV summarizes the study's conclusions and key findings.

II. Co-simulation Dynamic Model

Figure 1 illustrates the steps of the methodology developed for obtaining the dynamic model of co-simulation. The circuit in Figure 1a represents the base circuit, composed of a Thévenin equivalent circuit that feeds an RLC load through a transmission line. This circuit was prepared for co-simulation by selecting bus B1 as the interface bus, as depicted in Figure 1b. The Detailed System (DS), modeled in the EMT domain, includes the transmission line and the passive RLC load. Conversely, the External System (ES), modeled in the TS domain, incorporates the Thévenin equivalent circuit of a large-scale network. For simplicity, voltage and current sources were adopted as the equivalent circuits, respectively. Figure 1c illustrates the functional block diagram of the EMT-TS co-simulation. In the green rectangle labeled phasor-wave, the model of the phasor extraction method, based on DFT, LSCF, or SOGI-TVP, is included. Meanwhile, the small red rectangles represent communication delays between the EMT and TS programs.

A. Full-EMT model

From Figure 1a, one can formulate the following state-space representation as follows:

$$\dot{\mathbf{x}} = \begin{bmatrix} -\frac{R_t}{L_t} & 0 & -\frac{1}{L_t} & 0 \\ 0 & -\frac{R_t}{L_t} & 0 & -\frac{1}{L_t} \\ \frac{1}{C} & 0 & 0 & 0 \\ 0 & \frac{1}{C} & 0 & 0 \end{bmatrix} \mathbf{x} + \begin{bmatrix} \frac{1}{L_t} & 0 \\ 0 & \frac{1}{L_t} \\ 0 & 0 \\ 0 & 0 \end{bmatrix} \mathbf{u} \quad (1)$$

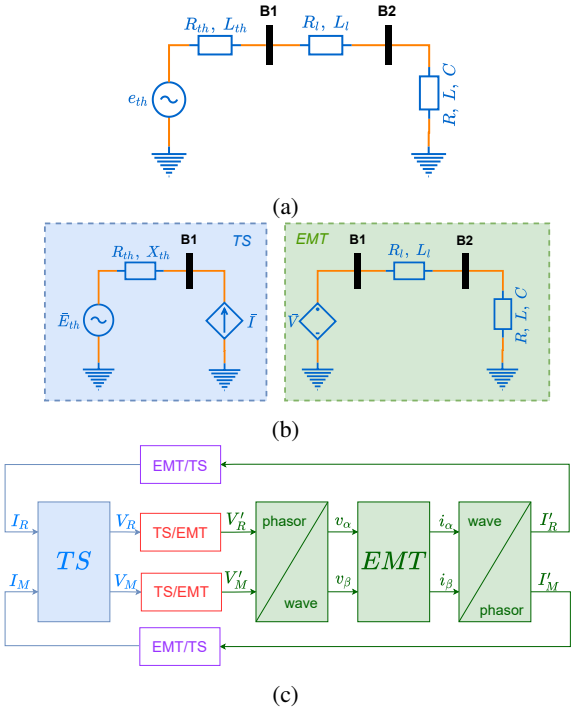

Fig. 1: Modeling steps of EMT–TS: (a) complete circuit (on EMT or TS); (b) split circuit for EMT–TS co-simulation; (c) dynamic model of the complete co-simulation.

where where $R_t = (R_{th} + R_\ell + R)$, $L_t = (L_{th} + L_\ell + L)$, $\dot{\mathbf{x}} = \begin{bmatrix} i_\alpha(t) & i_\beta(t) & v_{c,\alpha}(t) & v_{c,\beta}(t) \end{bmatrix}^\intercal$, $\mathbf{u} = \begin{bmatrix} e_\alpha(t) & e_\beta(t) \end{bmatrix}^\intercal$, and the superscript $(^\intercal)$ denotes transposed vector.

The model given in (1) is used to perform the complete Electromagnetic Transients (EMT) simulation of the system and compare with the results obtained from the EMT-TS co-simulation.

B. Co-simulation model

Considering Figure 1b, the TS equivalent circuit can be modeled as follows:

$$\overline{V}(t) = \overline{E}_{th}(t) - Z_{th}\overline{I}(t) \quad (2)$$

where $\overline{V}(t) = V_R(t) + jV_M(t)$ and $\overline{I}(t) = I_R(t) + jI_M(t)$ are, respectively, the time-varying phasors of voltage and current at the interface bus, and $\overline{E}_{th}(t) = E_R(t) + jE_M(t)$ is the phasor of the equivalent Thévenin voltage. The subscripts $(_R)$ and $(_M)$ denote the real and imaginary parts of the phasors, respectively.

Rewriting (2) in matrix form as follows:

$$\begin{bmatrix} V_R(t) \\ V_M(t) \end{bmatrix} = \begin{bmatrix} E_R(t) \\ E_M(t) \end{bmatrix} - \begin{bmatrix} R_{th} & -X_{th} \\ X_{th} & R_{th} \end{bmatrix} \begin{bmatrix} I_R(t) \\ I_M(t) \end{bmatrix} \quad (3)$$

The TS program is executed with a step H, typically in the order of milliseconds. In this study, the TS model is simplified by excluding associated dynamics. In real co-simulation scenarios, slow dynamics related to machine inertia will be a factor to consider.

1) Phasor-wave convertion: Referring to Figure 1b, the phasor voltage from the TS requires conversion into an instantaneous waveform in the EMT. This results in a wave represented by its real and imaginary components, as follows:

$$v(t) = \sqrt{2}V_R(t)\cos(\omega_o t) - \sqrt{2}V_M(t)\sin(\omega_o t) \tag{4}$$

where $v(t)$ is the reconstructed voltage waveform at the interface bus on the EMT side, $\overline{V}(t)$ is the phasor voltage at the interface bus coming from the TS.

The phasor-to-waveform conversion is a specific case of transforming from synchronous (dq) to stationary $\alpha\beta$ coordinates and can be expressed as follows:

$$\begin{bmatrix} v_\alpha(t) \\ v_\beta(t) \end{bmatrix} = \mathbf{T} \begin{bmatrix} V_R(t) \\ V_M(t) \end{bmatrix} \tag{5}$$

where,

$$\mathbf{T} = \begin{bmatrix} \cos\theta & -\sin\theta \\ \sin\theta & \cos\theta \end{bmatrix} \tag{6}$$

being $\theta = \omega_o t$.

Furthermore, any variation in the angular frequency of the transformed signal, denoted as ω_o, will be mirrored in the phase of the phasor $\overline{V}(t)$.

2) DFT and LSCF model: The DFT phasor extraction can be viewed as a sliding window of width equal to one fundamental cycle T_o, and a sampling frequency of $f_s = (1/T_s)$, as follows [9],

$$F_R(t) = \frac{2}{N}\sum_{k=0}^{N-1} f[k]\cos\left(\omega_o\left(t-(N-1-k)\right)\right) \tag{7a}$$

$$F_M(t) = -\frac{2}{N}\sum_{k=0}^{N-1} f[k]\sin\left(\omega_o\left(t-(N-1-k)\right)\right) \tag{7b}$$

where N is the number of samples, and $\overline{F}(t) = F_R(t) + jF_M(t)$ is the phasor.

The magnitude and angle of a generic phasor can be extracted using an algorithm based on the LSCF method by minimizing the error between the instantaneous signal and a standard curve. This is achieved by sampling the time-varying signal with a fixed number of samples over one fundamental period, as follows:

$$\varepsilon = \min\left\{\sum_{k=0}^{N-1}\left(f_k - c(k,\Gamma)\right)\right\} \tag{8}$$

where N is the number of samples of the instantaneous signal.

The goal is to find the parameters $\Gamma = \{I, \theta_I\}$ in the most common fitting curve given by:

$$c(k,\Gamma) = \sqrt{2}I\cos\left(\omega_0 t[k] + \theta_I\right) \tag{9}$$

If the fitting curve seeks amplitude and average phase, both the DFT and LSCF algorithms will yield the same result. Assuming that the microstep size h is exceedingly small, the EMT circuit can be approximated as continuous-time, allowing one to express (7a) and (7b) in the frequency domain as follows:

$$I_R(s) = 2\mathcal{L}\left\{i_\alpha(t)\cos\theta\right\}T_{sw}(s) \tag{10a}$$

$$I_M(s) = 2\mathcal{L}\left\{-i_\alpha(t)\sin\theta\right\}T_{sw}(s) \tag{10b}$$

where $\mathcal{L}\{\cdot\}$ is the Laplace transform operator, $i_\alpha(t)$ is the current, and $T_{sw}(s)$ is the transfer function of the sliding window,

$$T_{sw}(s) = \left(\frac{1-e^{-sT_o}}{sT_o}\right) \tag{11}$$

where $T_o = 1/f_o$ is the fundamental period of the extracted phasor, typically $f_o = 50$ or 60 Hz. It is worth emphasizing that both the DFT and the LSCF require historical data, and the transfer function (11) incorporates such dynamic behavior.

Writing (10a), (10b), and (11), in matrix representation:

$$\begin{bmatrix} I'_R(t) \\ I'_M(t) \end{bmatrix} = \left\{\begin{bmatrix} 2T_{sw}(t) & 0 \\ 0 & 2T_{sw}(t) \end{bmatrix}\right\} * \left\{\mathbf{T}\begin{bmatrix} i_\alpha(t) \\ i_\beta(t) \end{bmatrix}\right\} \tag{12}$$

where the operator $*$ represents convolution.

3) SOGI-TVP model: Figure 2 shows the block diagram of the Second-Order Generalized Integrator-Time Varying Phase-locked loop (SOGI-TVP), from which the transfer functions $D(s)$ and $Q(s)$ can be derived [4]:

$$D(s) = \frac{A_\alpha(s)}{A(s)} = \frac{k\widehat{\omega}\ s}{s^2 + k\widehat{\omega}\ s + \widehat{\omega}^2}, \tag{13a}$$

$$Q(s) = \frac{A_\beta(s)}{A(s)} = \frac{k\widehat{\omega}^2}{s^2 + k\widehat{\omega}\ s + \widehat{\omega}^2}, \tag{13b}$$

where $\widehat{\omega}$ is the angular frequency tracked by the Phase-Locked-Loop (PLL), k is the damping factor, which in many applications is made constant.

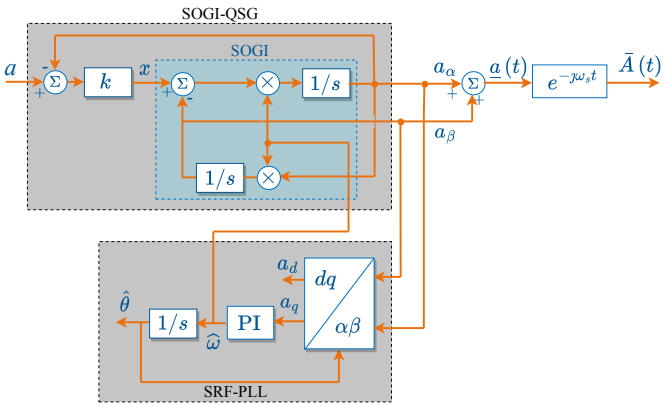

Fig. 2: Block diagram of SOGI-TVP.

From (13a) and (13b), it can be shown that the frequency shift $\varepsilon\{\cdot\} = \{\cdot\}e^{-j\omega_s t}$ can be viewed as a transformation $\alpha\beta \rightarrow dq$. Then, the following relationships for the real and imaginary parts of the current $i_\alpha(t)$ can be written:

$$\begin{bmatrix} I'_\alpha(s) \\ I'_\beta(s) \end{bmatrix} = \begin{bmatrix} D(s) \\ Q(s) \end{bmatrix} I_\alpha(s) \tag{14a}$$

$$\begin{bmatrix} I'_R(t) \\ I'_M(t) \end{bmatrix} = \begin{bmatrix} \cos\theta & \sin\theta \\ -\sin\theta & \cos\theta \end{bmatrix} \begin{bmatrix} i'_\alpha(t) \\ i'_\beta(t) \end{bmatrix} \tag{14b}$$

where $I'_R(t)$ and $I'_M(t)$ are, respectively, the real and imaginary parts of the extracted phasor, $i_\alpha(t)$ and $i_\beta(t)$ are the input currents in the α and β coordinates, $D(s)$ and $Q(s)$ are the transfer functions of the currents $i'_\alpha(t)$ and $i'_\beta(t)$ in terms of the current $i_\alpha(t)$.

4) Communication effects - extrapolation: Two effects must be modeled: (i) data extrapolation between communication instants, and (ii) time delay due to the nature of the communication protocol.

Due to significant difference in the micro-steps used between TS and EMT it is possible to mathematically model EMT in continuous time, while TS can be modeled in discrete time. Additionally, input signals at the interface bus must be extrapolated between two consecutive communication instants. In this work, a Zero order holder (ZOH) is used to represent the extrapolation effect. The ZOH introduces magnitude and phase errors in the signal, and its transfer function is given by:

$$T_{zoh}(s) = \left(\frac{1 - e^{-sM}}{sM}\right) \tag{15}$$

It is common to make the macro-step identical to the TS step, i.e., $M = H$, consequently the EMT signal sent to the TS undergoes no extrapolation. The block diagram in the Figure 3b shows such case, where the continuous-line red blocks model the extrapolation effect.

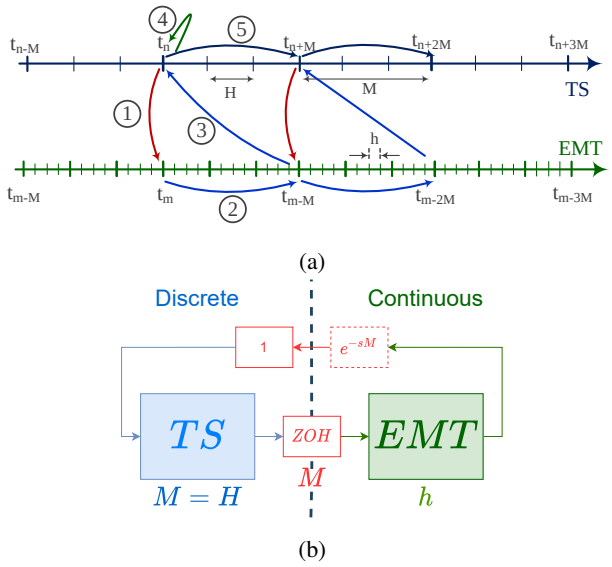

Fig. 3: Extrapolation and sampling due to communication: (a) timeline of the serial protocol, (b) block diagram of the EMT-TS co-simulation considering the extrapolation and protocol effects.

5) Communication effects - protocol: During co-simulation, the communication protocol introduces delays which must be included in the model. This work considers the serial protocol with TS priority, Figure 3a, as this is the most commonly found in the literature. The upper timeline is linked to TS, while the lower one is related to EMT. The TS to EMT has no time delay, while the EMT to TS always has a delay of one macro-step, denoted as M, due to the serial communication process.

The equation for the transport delay in the time of one macro-step, denoted as M, is given in the Laplace domain as:

$$T_{D,M}(s) = e^{-sM} \tag{16}$$

Figure 4 presents a schematic diagram of the co-simulation in a generic manner, considering the effects of (i) data extrapolation between information exchange instants and (ii) time delay due to the adopted serial communication protocol as a reference.

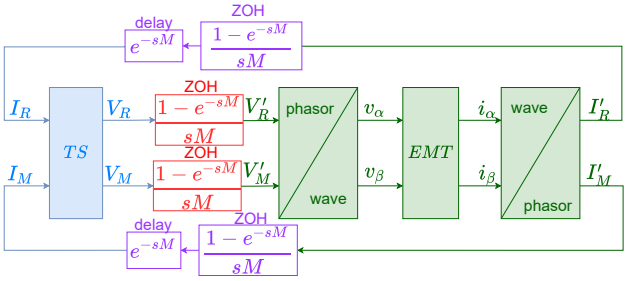

Fig. 4: Generic block diagram for the stability study of non-iterative EMT-TS co-simulation considering communication effects.

C. General Dynamic Model

It is possible to develop a generic approach of Figure 4 to obtain the state-space model for any type of phasor extraction. Considering that the EMT part in Figure 4 always has the form,

$$\begin{bmatrix} \dot{i}_\alpha(t) \\ \dot{i}_\beta(t) \\ \dot{v}_\alpha(t) \\ \dot{v}_\beta(t) \end{bmatrix} = \left[\begin{array}{c|c} \mathbf{A_{11}} & \mathbf{A_{1,234}} \end{array}\right] \begin{bmatrix} i_\alpha(t) \\ i_\beta(t) \\ v_\alpha(t) \\ v_\beta(t) \end{bmatrix} + \mathbf{B_1} \begin{bmatrix} v_\alpha(t) \\ v_\beta(t) \end{bmatrix} \tag{17}$$

where,

$$\mathbf{A_{1,1}} = \begin{bmatrix} -\frac{R_t}{L_t} \\ 0 \\ \frac{1}{C} \\ 0 \end{bmatrix} \tag{18}$$

$$\mathbf{A_{1,234}} = \begin{bmatrix} 0 & -\frac{1}{L_t} & 0 \\ -\frac{R_t}{L_t} & 0 & -\frac{1}{L_t} \\ 0 & 0 & 0 \\ \frac{1}{C} & 0 & 0 \end{bmatrix} \tag{19}$$

$$\mathbf{B_1} = \begin{bmatrix} \frac{1}{L_t} & 0 \\ 0 & \frac{1}{L_t} \\ 0 & 0 \\ 0 & 0 \end{bmatrix} \tag{20}$$

On the other hand, the TS in Figure 4 can be written in the stationary framework $\alpha\beta$, pre-multiplying (3) by (6) as shown below:

$$\mathbf{T}\begin{bmatrix} V_R(t) \\ V_M(t) \end{bmatrix} = \mathbf{T}\left(\begin{bmatrix} E_R(t) \\ E_M(t) \end{bmatrix} - \begin{bmatrix} R_{th} & -X_{th} \\ X_{th} & R_{th} \end{bmatrix}\begin{bmatrix} I_R(t) \\ I_M(t) \end{bmatrix}\right) \tag{21}$$

which can be written as follows,

$$\begin{bmatrix} v_\alpha(t) \\ v_\beta(t) \end{bmatrix} = \begin{bmatrix} e_\alpha(t) \\ e_\beta(t) \end{bmatrix} - \begin{bmatrix} \Delta v_\alpha(t) \\ \Delta v_\beta(t) \end{bmatrix} \tag{22}$$

The dynamics of (i) TS, (ii) communication, and phasor-wave transformation of Figure 4, always have the form,

$$\begin{bmatrix} \Delta v_\alpha(t) \\ \Delta v_\beta(t) \end{bmatrix} = \mathbf{T}\left\{\begin{bmatrix} P(t) & -Q(t) \\ Q(t) & P(t) \end{bmatrix}\right\} * \left\{\mathbf{T}^{-1}\begin{bmatrix} i_\alpha(t) \\ i_\beta(t) \end{bmatrix}\right\} \tag{23}$$

where $P(t)$ and $Q(t)$ are dynamics on the synchronous side due to communication and phasor extraction methods.

The stationary reference frame was chosen due to the simplicity of the resulting equation model. Thus, (23) can be written in the frequency domain as follows,

$$\begin{bmatrix} \Delta V_\alpha(s) \\ \Delta V_\beta(t) \end{bmatrix} = \begin{bmatrix} P'(s) & -Q'(s) \\ Q'(s) & P'(s) \end{bmatrix}\begin{bmatrix} I_\alpha(t) \\ I_\beta(t) \end{bmatrix} \tag{24}$$

where,

$$\begin{aligned} P'(s) = \frac{1}{2}\Big[P(s+j\omega_o) + P(s-j\omega_o)\Big] + \\ \frac{1}{2}\Big[-jQ(s+j\omega_o) + jQ(s-j\omega_o)\Big] \end{aligned} \tag{25}$$

$$\begin{aligned} Q'(s) = \frac{1}{2}\Big[jP(s+j\omega_o) - jP(s-j\omega_o)\Big] + \\ \frac{1}{2}\Big[Q(s+j\omega_o) + Q(s-j\omega_o)\Big] \end{aligned} \tag{26}$$

$P(s)$ and $Q(s)$ are transfer functions that contain transport delays and, therefore, are transcendental functions. Padé approximations of various orders can be performed, with the most common ones being first and second order. Writing (24) in state-space form yields,

$$\dot{\mathbf{x}} = \mathbf{A_2}\mathbf{x} + \mathbf{B_2}i_\alpha \tag{27a}$$

$$\mathbf{\Delta v}_{\alpha\beta} = \mathbf{C_2}\mathbf{x} + \mathbf{D_2}i_\alpha \tag{27b}$$

where $\dot{\mathbf{x}}$ is the state vector with n elements, $\mathbf{A_2}$ is the state matrix, $\mathbf{B_2}$ is the input matrix, $\mathbf{C_2}$ is the output matrix, and $\mathbf{D_2}$ is the direct transfer matrix.

If a second-order Padé approximation is used, for instance, $\mathbf{A_2}$ will be a 4×4 matrix. This occurs because the second-order approximation introduces 4 poles into the system, 2 from $P(s)$ and 2 from $Q(s)$.

Substituting (27b) em (22) and concatenating (17) with (27a), yields:

$$\begin{bmatrix} \dot{i}_\alpha(t) \\ \dot{i}_\beta(t) \\ \dot{v}_\alpha(t) \\ \dot{v}_\beta(t) \\ \hdashline \dot{\mathbf{x}} \end{bmatrix} = \mathbf{A}\begin{bmatrix} i_\alpha(t) \\ i_\beta(t) \\ v_\alpha(t) \\ v_\beta(t) \\ \hdashline \mathbf{x} \end{bmatrix} + \mathbf{B}\begin{bmatrix} e_\alpha(t) \\ e_\beta(t) \end{bmatrix} \tag{28}$$

where

$$\mathbf{A} = \left[\begin{array}{c|c|c} (\mathbf{A_{1,1}} + \mathbf{B_1}\mathbf{D_2}) & \mathbf{A_{1,234}} & -\mathbf{B_1}\mathbf{C_2} \\ \hline \mathbf{B_2} & \mathbf{Z_1} & \mathbf{A_2} \end{array}\right] \tag{29}$$

$$\mathbf{B} = \begin{bmatrix} \mathbf{B_1} \\ \hdashline \mathbf{Z_2} \end{bmatrix} \tag{30}$$

where $\mathbf{Z_1}$ is the zero-matrix with n rows and 3 columns; and $\mathbf{Z_2}$ is the zero matrix with n rows and 2 columns.

D. Developed models

To proceed with the co-simulation stability analysis, the following models were constructed:

Model A: DFT without communication.
Model B: SOGI-TVP without communication.
Model C: DFT with communication.
Model D: SOGI-TVP with communication.

III. Results

This section presents the results of the proposed methodology, including eigenvalue analyses, map of poles and zeros, voltage profiles and system behavior under different operating conditions. The main parameters of the electrical system are summarized below:

- three buses, 230 kV / 77.62 MVA;
- one transmission line of 160 km (Table I);
- RLC load: $S_{3\phi} = (75 + j30)$ MVA or $\overline{Z}_L = (235.1111 + j587.7778)\ \Omega$;
- Thévenin equivalent impedance: $\overline{Z}_{th} = (2.6450 + j26.4648)\ \Omega$;
- Three-phase short-circuit between 0.5 and 0.6 s with zero impedance at bus 1.

TABLE I: Line parameters per unit length.

Parameter	Unit	Value (pos. and neg.)	Value (zero)
r	Ω/km	0.050	0.050
ℓ	H/km	1.2944×10^{-3}	3.8832×10^{-3}
c	F/km	8.9418×10^{-9}	4.4709×10^{-9}

The developed dynamic models will only consider the positive sequence component of the signals. Thus, in order to simplify the modeling, a single-phase equivalent system will be used in the co-simulations. Additionally, the effect of line capacitance has been neglected.

A. Sensitivity of the Thevenin Equivalent Circuit

The Figure 5 illustrates how the circuit stability is affected by the variation of the Thevenin equivalent circuit parameters on the TS side. The x and y axes represent the variations of X_{th} and R_{th}, while the z-axis represents the pole with the highest real part associated, among all poles in the co-simulation. The formed surfaces are related to models A, B, C, or D. If the surface is negative on the z-axis, the co-simulation will be stable, as the pole will be in the left semi-plane. On the other hand, if the surface value is positive, the co-simulation will be unstable. For example, if $R_{th} = X_{th} = 4$ pu, the co-simulation will be unstable for all surfaces because the values on the z-axis are positive. As shown in Figure 5, weaker

systems exhibit a greater tendency towards instability during co-simulation. It is evident that false stability points may arise if communication effects are not considered. At point (1), the system is moderately strong ($SCR > 3$), and co-simulation remains stable for both models with and without communication, as seen in Figure 5 (a) and (b), respectively. However, at point (2), when communication is considered, both models with DFT and SOGI-TVP become unstable, highlighting the importance of communication modeling. On the other hand, at point (3), SOGI-TVP without communication seemed stable while DFT was unstable. Nevertheless, when communication modeling was incorporated, both were revealed to be unstable.

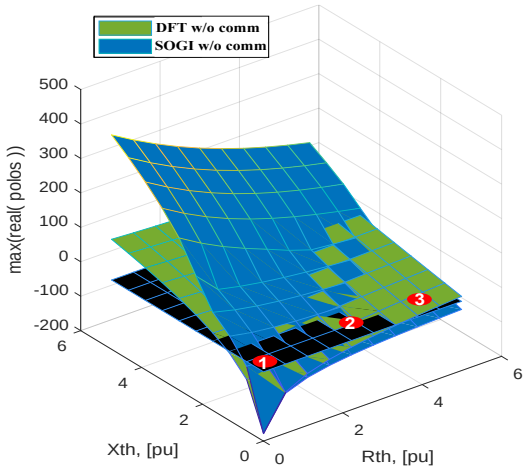

(a)

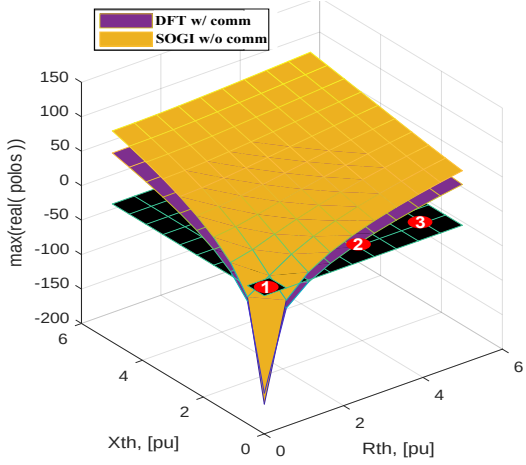

(b)

Fig. 5: The maximum real part value of the eigenvalues of the EMT-TS co-simulation for variations in R_{th} and X_{th} while all other values remain constant: (a) Models A and B; and (b) Models C and D.

B. Load Sensitivity

To investigate the impact of the power at the interface bus, a similar approach was taken by plotting the maximum real part value among the eigenvalues of the system. However, active and reactive powers were varied within the ranges of $0 < P_L < 2$ pu and $0 < Q_L < 2$ pu, respectively. Figure 6 demonstrates that the system remains stable for large ranges of power at the interface bus, considering the system with nominal data, i.e., a very strong system with $SCR = 26.52$. However, for low active powers, the system tends toward instability with positive eigenvalues for all models.

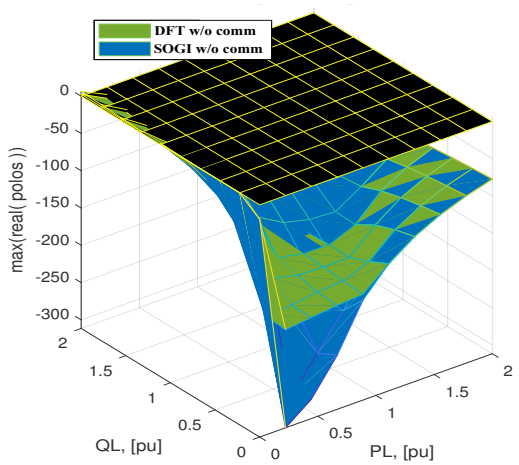

(a)

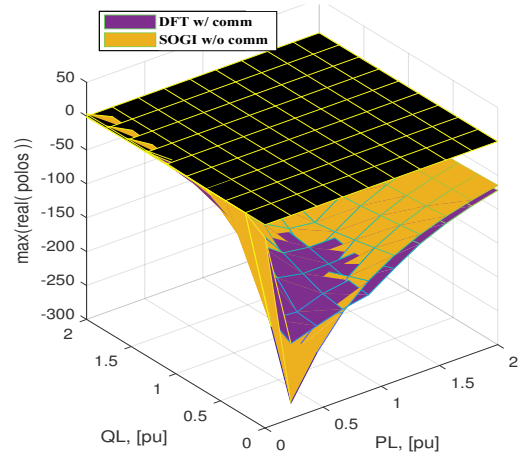

(b)

Fig. 6: The maximum real part value of the eigenvalues of the EMT-TS co-simulation for variations in R_{th} and X_{th} while all other values remain constant: (a) Models A and B; and (b) Models C and D.

To validate this prediction, an operating point with low active power was chosen. Figure 7 (a) displays the eigenvalues of models C and D using the second-order Padé approximation when $P_L = 0$ pu. The four eigenvalues of the full-EMT system are $-0.97225 \pm j232.31$, and they are not depicted on the graph due to scale limitations. As observed, the models predicted that the co-simulation with the SOGI-TVP method would be unstable and with the DFT method would be stable. To validate this claim, the system was co-simulated using both extraction methods, and the voltage results at the interface bus are shown in Figure 7 (b). It can be observed that both voltages

remain stable until the fault application. However, after 0.5 seconds, case D diverges and becomes unstable, confirming the stability prediction of the model. On the other hand, case C remains stable after the fault. It is worth noting that accuracy at extreme operating points may be compromised due to the approximations.

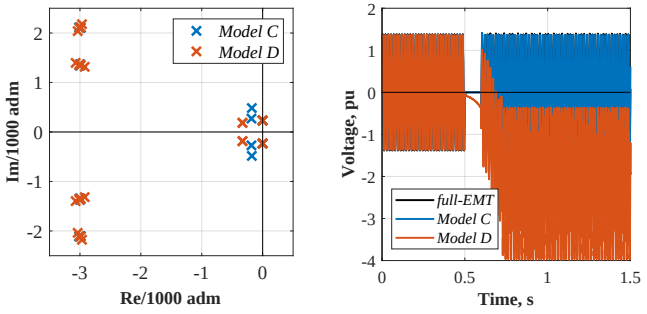

(a) (b)

Fig. 7: Low active power: evaluation of $P_L = 0$ pu on the stability of EMT-TS co-simulation, primarily based on the operating point: (a) eigenvalues of Models C and D; and (b) voltages at the interface bus.

C. Effect of the DC Component

In the SOGI-TVP, the transfer functions of the components $A_\alpha(s)$ and $A_\beta(s)$ with respect to the input $A(s)$ exhibit different behaviors, especially at low frequencies. The transfer function $G_\alpha(s)$ has a zero at the origin, implying that it provides zero gain at 0 Hz and therefore completely rejects the Direct Current (DC) component. Conversely, the gain of $G_\beta(s)$ at 0 Hz is equal to $G_\beta(s=0) = k$, amplifying the DC signal if it exists in the input signal $a(t)$. This section aims to investigate the behavior of the SOGI-TVP concerning the DC component and its stability.

The surface in Figure 8 illustrates the variation of active and reactive power in the model with SOGI-TVP for three systems: strong with $SCR = 26.534$, moderately weak with $SCR = 2.667$, and weak with $SCR = 1.333$, based on the variation of the X_{th}/R_{th} ratio. It can be observed that as the X_{th}/R_{th} ratio increases (or the system becomes weaker), the co-simulation of EMT-TS tends to become more unstable.

The SOGI-TVP can be enhanced by adding one or more origin zeros to $G_\beta(s)$. For this purpose, the Third-Order Generalized Integrator (TOGI), proposed by [18] due to its simplicity, was adopted, as depicted in Figure 9.

The transfer functions are as follows:

$$D(s) = \frac{k\omega s}{s^2 + k\omega s + \omega^2} \tag{31a}$$

$$Q'(s) = \frac{k\omega s}{s^2 + k\omega s + \omega^2}\left(\frac{\omega - s}{s + \omega}\right) \tag{31b}$$

The Figure 10 presents the eigenvalues of models C and D, as well as the eigenvalues of the system enhanced with the TOGI, using the 2nd order Padé approximation. The four

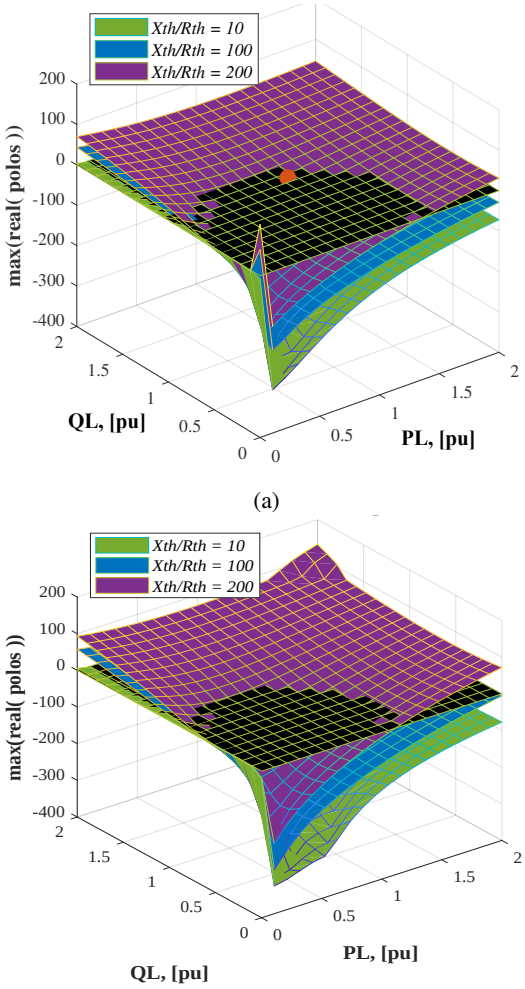

(a)

(b)

Fig. 8: Eigenvalue Surface for Model D for Analysis of the DC Component, considering $X_{th}/R_{th} = 10$, 100, and 200, i.e., weak-moderate systems with $SCR = 2.667$ and weak systems with $SCR = 1.333$, respectively: (a) Model D and (b) Model D'.

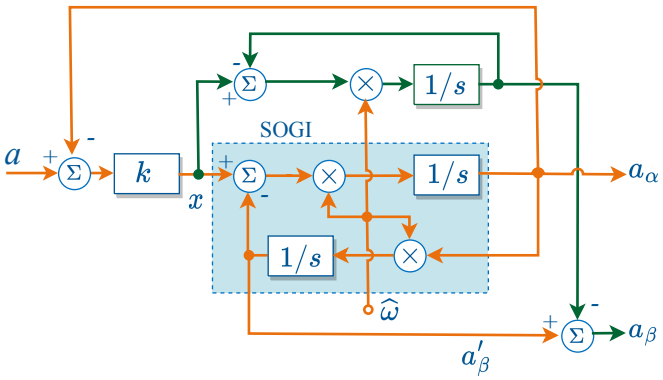

Fig. 9: TOGI Topology for DC Component Rejection.

eigenvalues of the full-EMT system are $-88.625 \pm j135.41$, and they are not depicted on the graph due to scale limi-

tations. For this purpose, the Thévenin equivalent circuit is not nominal, with $R_{th} = 2.645\ \Omega$ and $X_{th} = 529.000\ \Omega$, characterizing a weak interface bar $SCR = 1.3333$. The models predicted that co-simulation with SOGI-TVP would be unstable, and in the case of filtering the DC component, co-simulation would become stable. Therefore, it is expected to confirm these conclusions. Conducting the co-simulation, Figure 10 (b) shows the voltages at the interface bar. Note that the voltages for Model C and D' remain stable throughout the simulation. However, the voltage of Model D becomes unstable after 0.1 s. Consequently, it can be concluded that the developed model correctly predicted the stability of the EMT–TS co-simulation for the operating point.

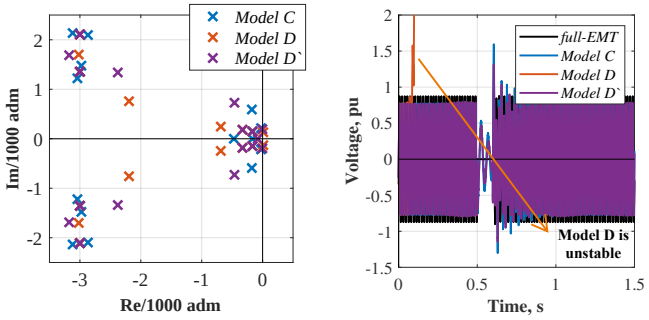

(a) (b)

Fig. 10: Assessment of the Effect of the DC Component: (a) eigenvalues of Models C, D, and D'; and (b) voltages at the interface bus.

D. Effect of Communication

According to Figure 5, at point (2), Model A, without considering communication, predicted co-simulation to be stable, while Model C, considering communication, predicted it to be unstable. Thus, this section assesses the effect of communication on co-simulation stability. For this purpose, the Thévenin equivalent circuit has $R_{th} = 705.330\ \Omega$ and $X_{th} = 3526.700\ \Omega$, characterizing a weak interface bar ($SCR = 0.20$). Similarly, Models D and D' also predict instability. Therefore, it is expected to confirm that considering communication in the models is essential for consistent modeling.

Figure 11(a) shows the eigenvalues of Models C and D' for co-simulation using the 2nd order Padé approximation. The four eigenvalues of the full-EMT system are $-56.318 \pm j63.076$, and they are not depicted on the graph due to scale limitations. Note that for both models, it predict co-simulation to be unstable, even with relatively small negative real parts. In addition, Figure 11(b) displays the voltages at the interface bar for co-simulation. Observe that the voltages for cases C and D' are unstable. Thus, it can be concluded that the developed model correctly predicted the stability of the EMT–TS co-simulation for the operating point, emphasizing the importance of considering communication in the models.

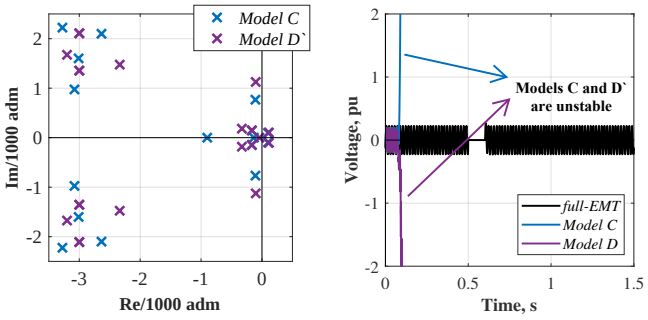

(a) (b)

Fig. 11: Assessment of the effect of communication: (a) eigenvalues of Models C and D'; and (b) voltages at the interface bus.

IV. Conclusion

This work has presented an investigation into the stability of co-simulation, considering the phasor extraction method and communication effects. Three phasor extraction techniques and methods used in the EMT-TS co-simulation interface were modeled and compared. The developed models were validated using dynamic simulations in the time domain, performed in a non-iterative manner using the Matlab/Simulink environment with the SimPowerSystems library.

Through the dynamic models developed, the main parameters and characteristics that are most likely to allow stable co-simulation were identified. The results indicate that a strong interface bar has a higher tendency towards stability. Moreover, extreme power values (much higher or lower than the nominal power) can lead to instability. Additionally, the choice of macro time step values must be made carefully to avoid entering regions of instability.

The developed models show that the DC component of the phasor extracted by SOGI-TVP must be filtered to achieve a wider stable operating range in co-simulation. Furthermore, including modeling for the effects of sampling and interface delay is crucial for accurate analyses, as neglecting them can lead to false stable co-simulation points.

The methods can be considered stable for most practical applications with moderately-strong interface bars. Although DFT exhibits a larger stability region for extremely weak systems, its practical application is limited. Therefore, in cases where the interface bars are very weak, the use of DFT as a phasor extraction method may be more suitable. On the other hand, for moderately-strong systems, SOGI-TVP may be more appropriate due to its precision and stability.

Although not within the scope of this work, the methodology can be extended to encompass more complex systems, incorporating electric machines, mechanical loads, control laws, stability verification, phasor extraction methods, and communication protocols. The challenges associated with increasing system complexity primarily revolve around equation formulation. However, these obstacles can be overcome

through automation facilitated by symbolic equation-solving tools.

The potential contribution of this work relates to the proposed co-simulation stability study methodology. It proved to be adequate through numerical validation, and it demonstrated that phasor extraction methods and/or communication protocols can make simulations unstable for a naturally stable system if the interface bar or communication step is chosen inappropriately. In this context, the proposed methodology is generic and can be used to assess the stability of other phasor extraction methods, communication protocols, or more complex systems, contributing to further research and advancements in co-simulation technology.

REFERENCES

[1] J. M. Smith, K. Balasubramaniam, and R. Hadidi, "Assessing the need and state of power system and transportation system co-simulation," *IEEE Access*, 2023.

[2] P. Palensky, A. A. Van Der Meer, C. D. Lopez, A. Joseph, and K. Pan, "Co-simulation of intelligent power systems, part i and ii," *IEEE Industrial Electronics Magazine*, 2017.

[3] D. Shu, X. Xie, V. Dinavahi, C. Zhang, X. Ye, and Q. Jiang, "Dynamic phasor based interface model for EMT and transient stability hybrid simulations," *IEEE Transactions on Power Systems*, vol. 33, no. 4, pp. 3930–3939, 2017.

[4] T. S. Theodoro, M. A. Tomim, P. G. Barbosa, A. C. Lima, and M. T. C. de Barros, "A flexible co-simulation framework for penetration studies of power electronics based renewable sources: A new algorithm for phasor extraction," *International Journal of Electrical Power & Energy Systems*, vol. 113, pp. 419–435, 2019.

[5] R. Sadnan, G. Krishnamoorthy, and A. Dubey, "Transmission and distribution (t&d) quasi-static co-simulation: Analysis and comparison of t&d coupling strength," *IEEE Access*, vol. 8, pp. 124 007–124 019, 2020.

[6] A. Thakallapelli, S. Ghosh, and S. Kamalasadan, "Development and applicability of online passivity enforced wide-band multi-port equivalents for hybrid transient simulation," *IEEE Transactions on Power Systems*, vol. 34, no. 3, pp. 2302–2311, 2018.

[7] A. Constantin, A. Ellerbrock, F. Fernandez *et al.*, "Co-simulation of power electronic dominated networks," *IEEE Power and Energy Magazine*, vol. 18, no. 2, pp. 84–89, 2020.

[8] E. Buraimoh, G. Ozkan, L. Timilsina, P. K. Chamarthi, B. Papari, and C. S. Edrington, "Overview of interface algorithms, interface signals, communication and delay in real-time co-simulation of distributed power systems," *IEEE Access*, 2023.

[9] Z. Yu, "Dynamic modeling, design and control of power converters for renewable interface and microgrids," Ph.D. dissertation, Arizona State University, 2018.

[10] R. Brandl, "Operational range of several interface algorithms for different power hardware-in-the-loop setups," *Energies*, vol. 10, no. 12, p. 1946, 2017. [Online]. Available: https://www.mdpi.com/1996-1073/10/12/1946

[11] F. Plumier, "Co-simulation of electromagnetic transients and phasor models of electric power systems," Ph.D. dissertation, Université de Liège, Liège, Belgium, 2016.

[12] J. Rupasinghe, S. Filizadeh, and K. Strunz, "Assessment of dynamic phasor extraction methods for power system co-simulation applications," *Electric Power Systems Research*, vol. 197, p. 107319, 2021.

[13] V. Venkatasubramanian, "Tools for dynamic analysis of the general large power system using time-varying phasors," *International Journal of Electrical Power & Energy Systems*, vol. 16, no. 6, pp. 365–376, 1994.

[14] S. R. Sanders, J. M. Noworolski, X. Z. Liu, and G. C. Verghese, "Generalized averaging method for power conversion circuits," *IEEE Transactions on power Electronics*, vol. 6, no. 2, pp. 251–259, 1991.

[15] S. Henschel, "Analysis of electromagnetic and electromechanical power system transients with dynamic phasors," Ph.D. dissertation, University of British Columbia, 1999.

[16] K. Mudunkotuwa, S. Filizadeh, and U. Annakkage, "Development of a hybrid simulator by interfacing dynamic phasors with electromagnetic transient simulation," *IET Generation, Transmission & Distribution*, vol. 11, no. 12, pp. 2991–3001, 2017.

[17] C. Zhang, X. Zhao, X. Wang, X. Chai, Z. Zhang, and X. Guo, "Comparative performance of three phasor-extraction algorithms for co-simulation of electrical power systems," *Journal of Control, Automation and Electrical Systems*, pp. 1–13, 2022.

[18] ——, "A grid synchronization pll method based on mixed second-and third-order generalized integrator for dc offset elimination and frequency adaptability," *IEEE Journal of Emerging and Selected Topics in Power Electronics*, vol. 6, no. 3, pp. 1517–1526, 2018.